

Surface abundance and the hunt for stratification in chemically peculiar hot subdwarfs: PG 0909+276 and UVO 0512–08

J. F. Wild^{1,2} and C. S. Jeffery^{1,3}

¹*Armagh Observatory and Planetarium, College Hill, Armagh BT61 9DG, N. Ireland*

²*Department of Physics & Astronomy, University of Sheffield, Sheffield, S3 7RH, UK*

³*School of Physics, Trinity College Dublin, Dublin 1, Republic of Ireland*

Received September 5, 2017

ABSTRACT

Edelmann (2003) identified two chemically peculiar hot subdwarfs, PG 0909+276 and UVO 0512–08, as having very high overabundances of iron-group elements. We obtained high-resolution ultraviolet spectroscopy in order to measure abundances of species not observable in the optical, and to seek evidence for chemical stratification in the photosphere. Abundances were measured in three wavelength regions; the optical 3900Å–6900Å range was re-analysed to confirm consistency with Edelmann (2003). Ultraviolet spectra were obtained with the Space Telescope Imaging Spectrograph (STIS) on the Hubble Space Telescope (HST), covering the far-UV (1140Å–1740Å) and the near-UV (1740Å–2500Å). We computed a grid of theoretical LTE spectra to find basic parameters (effective temperatures, surface gravity, surface hydrogen and helium fractions). We measured abundances using a spectral-synthesis approach in each wavelength range. We confirm that several iron-group metals are highly enriched, including cobalt, copper and zinc, relative to typical sdB stars. We detect gallium, germanium, tin, and lead, similar to analysis of ultraviolet spectra of some other sdB stars. Our results confirm that PG 0909+276 and UVO 0512–08 exhibit peculiarities which make them distinct from both the normal H-rich sdB and intermediate He-rich sdB stars. The process which leads to this particular composition has still to be identified.

Key words: stars: abundances – stars: fundamental parameters – stars: chemically peculiar – stars: individual (PG 0909+276) – stars: individual (UVO 0512–08) – stars: subdwarfs

1 INTRODUCTION

Hot subdwarfs form a class of compact, low-mass, evolved stars with very high surface temperatures. A subclass with spectral type B, having strong Balmer lines, weak neutral helium lines and no ionised helium lines, are known as sub-luminous B or sdB stars. These objects have masses $M < 0.5 M_{\odot}$, and typically consist of a helium burning core surrounded by a thin, inert hydrogen layer that is unable to sustain fusion. They have effective temperatures (T_{eff}) in the range 20 000 to 35 000 K and surface gravities $\log g/\text{cm s}^{-2}$ in the range 5.5 to 6.5, placing them on or near the blue end of the extreme horizontal branch on the Hertzsprung-Russell diagram (Heber 2016). The majority are extremely helium-poor. With T_{eff} up to 45 000 K, hot subdwarfs showing both neutral and ionised helium lines are known as sdOB stars; they show a range of helium abundances from helium-weak

though to extremely helium-strong. Most are located on or close to the helium main sequence.

The formation and evolution of hot subdwarfs is not fully understood, with one problem being the very large amount of mass loss required before the helium core ignites, and another being the number of subclasses observed. Several potential evolutionary tracks have been proposed, including a late helium flash in a post-giant star (Brown et al. 2001; Miller Bertolami et al. 2008), common-envelope binary evolution (Han 1998; Ivanova et al. 2013), or a white dwarf merger (Iben 1990; Saio & Jeffery 2002; Zhang & Jeffery 2012). However, it is difficult to say to which track a given hot subdwarf belongs.

In a previous analysis of high-resolution optical spectra, two sdOB stars PG 0909+276 and UVO 0512–08 were found to be hydrogen-weak, with peculiar super-solar abundances of metals with atomic number $Z \geq 7$ (Edelmann

2003; Geier 2013). Bright enough to observe at low resolution with the International Ultraviolet Observer *IUE*, new high-resolution ultraviolet spectra have been obtained with the Hubble Space Telescope (*HST*) in order to better determine the elemental composition of these two stars, including the identification of additional species.

It has been suggested in the analyses of other chemically peculiar, hydrogen-poor sdB stars (Naslim et al. 2013) that extreme overabundances of heavy elements are primarily due to enrichment of the stellar atmosphere by selective radiative levitation of specific ions such that these ions form layers (strata) of high concentration in the line forming region of the photosphere.

Since different lines probe different physical depths depending on line strength and the local continuum, a secondary goal is to find evidence for chemical stratification within the photosphere. However, because the difference in line formation depths is only a tiny fraction of a typical sdB radius, this is a challenging goal.

Third, the question arises as to why these stars contain a substantially larger fraction of heavy metals than other similar hot subdwarfs (O’Toole 2004). A possible solution is that heavier metals, due to their more complex electron configuration, have more spectral lines that could intercept and absorb a larger fraction of high-energy photons. This makes them more susceptible to radiative levitation than light ions with simpler outer electron structures. Evidence for chemical stratification in the photosphere could support this idea.

This paper summarizes the observations used (§2), as well as the models and methods used to analyse the data (§3). We determine the basic parameters and photospheric abundances for each star, in particular comparing results obtained in different wavelength regions (§4.5). The results and their potential implications are discussed in the context of previously observed hot subdwarfs (§6).

2 OBSERVATIONS

We use data from three sets of observations: high-resolution ultraviolet spectra from the Space Telescope Imaging Spectrograph (STIS), low-resolution ultraviolet spectrophotometry from *IUE*, and high-resolution optical spectra from the Fiber-Optics Cassegrain Echelle Spectrograph (FOCES) mounted on the 2.2m telescope of the Deutsch-Spanisches Astronomisches Zentrum at the Calar Alto Observatory, Spain. The latter were obtained and analysed by Edelmann (2003); Geier (2013). Details are given in Table 1.

For both stars, optical spectra show large sections that have either weak or no lines, although Edelmann (2003) notes that the optical spectrum of UVO 0512–08 contains many more lines than expected from a hot subdwarf. With several strong hydrogen and helium lines, and isolated lines of other species, the optical spectra provide the most robust means to determine basic parameters and to estimate abundances of some key elements.

Data were obtained with the *HST* in both the near ultraviolet (NUV) and far ultraviolet (FUV). Reduced data from the pipeline provided by Space Telescope Science Institute were obtained from the online archive. PG 0909+276

was also observed with *HST*/STIS by Rauch in March 2017. These data are still proprietary at the time of writing.

The FUV is particularly crowded with blended absorption lines, with neither star showing any regions that are clearly continuum. Significant line blending makes normalization of this region a challenge, as it is unclear where the continuum should be set. In order to obtain a spectrum for which analysis was possible, it was assumed that the highest level fluxes observed approximately represent the continuum and the spectrum was rectified accordingly. The normalization represents a potential source of systematic error which can be assessed when comparing results for different wavelength regions.

The NUV presents slightly fewer lines, as well as having some sections of continuum spectrum. This allows for much easier normalization. Additionally, the atomic data for this region are more complete than for the FUV.

We verified the radial and projected rotational velocities v_{rad} , $v_{\text{rot}} \sin i$ of each star from the optical spectra. For PG 0909+276, we found $v_{\text{rad}} = 20.7 \text{ km s}^{-1}$ and $v_{\text{rot}} \sin i < 2 \text{ km s}^{-1}$. For UVO 0512–08, we found $v_{\text{rad}} = 11.7 \text{ km s}^{-1}$ and $v_{\text{rot}} \sin i < 2 \text{ km s}^{-1}$. The sharp metal lines are consistent with a microturbulent velocity that is less than 2 km s^{-1} in both stars. These values agree with results obtained using the same data by Edelmann (2003) and also reported by Martin et al. (2016).

We compare our final models with spectra obtained with *IUE*, to confirm our measurements of the stars’ T_{eff} match historic data. We use two of the four observations of UVO 0512–08 made by *IUE* on the 28th of February 1980. Specifically, we use the data for which the star was observed at low dispersion, using the large aperture of the instrument. The first observation covers the far ultraviolet, and the second covers the near ultraviolet. PG 0909+276 was observed with the same method, on the 7th of January 1986.

We also use photometric observations of both stars. We obtained 6 measurements of PG 0909+276 in the B, V, R, J, H, and K bands (Høg et al. 2000; Zacharias et al. 2009; Cutri et al. 2003) and 5 measurements of UVO 0512–08 in the B, V, J, H, and K bands (Høg et al. 2000; Cutri et al. 2003). These are considered in our fitting of the *IUE* data.

3 METHODS

Model atmospheres and theoretical spectra for fitting these to the observations were computed with LTE-CODES, a package which includes STERNE (Behara & Jeffery 2006), SPECTRUM (Jeffery et al. 2001a), LTE_LINES (Jeffery 1991) and SFIT (Jeffery et al. 2001b). These assume that the atmosphere is semi-infinite, plane parallel, and in radiative, hydrostatic, and local thermodynamic equilibrium (LTE).

The first stage of analysis is to generate a grid of model atmospheres with STERNE and creating a model grid with three varying parameters: effective temperature (T_{eff}), surface gravity (g), and helium fraction (by number: n_{He}), and assuming solar abundances for other elements¹. These mod-

¹ In its simplest mode, STERNE requires abundances for hydrogen, helium, carbon, nitrogen, oxygen, silicon, calcium and iron. The abundances of other elements are scaled to the abundances for calcium and iron.

Table 1. Observations

Star	Instrument	Date	R	$\lambda/\text{\AA}$	n	$t_{\text{exp/s}}$	S/N	Image
PG 0909+276	DSAZ FOCES	2000.01	30 000	3900 – 6900	3	5400	30	
	<i>HST</i> STIS E140M	2015.04.24	45 800	1140 – 1740	1	2989	20	OCKS02020
	<i>HST</i> STIS E230M	2015.04.24	30 000	1740 – 2500	1	2019	50	OCKS02010
	<i>IUE</i> SWP LORES LAP	1986.01.07	260	1150 – 2000	1	300		SWP27469LL
	<i>IUE</i> LWP LORES LAP	1986.01.07	320	1850 – 3350	1	450		LWP07464LL
UVO 0512–08	DSAZ FOCES	2000.01–02	30 000	3900 – 6900	2	7200	30	
	<i>HST</i> STIS E140M	2015.02.25	45 800	1140 – 1740	1	1006	20	OCKS01010
	<i>HST</i> STIS E230M	2015.02.25	30 000	1740 – 2500	1	696	30	OCKS01020
	<i>IUE</i> SWP LORES LAP	1980.02.28	260	1150 – 1950	1	235		SWP08075LL
	<i>IUE</i> LWR LORES LAP	1980.02.28	320	1900 – 3200	1	330		LWR07043LL

els are used as input to SPECTRUM to generate high resolution model spectra. SFIT compares these to the observed spectrum to obtain a first estimate for T_{eff} , g and n_{He} . Based on these estimates, SFIT is used to make a first estimate of abundances by adjusting the abundances of the most significant metals, namely C, N, O, Si, Ca and Fe. Based on these, a new model atmosphere grid is generated with STERNE and the process is iterated. A final STERNE model is computed with T_{eff} , g , n_{He} and major abundances based on these results, and the remaining metal abundances are measured from the observed spectrum using this model. The final composition is shown in Tables 3 and 5.

Evidence that the LTE approximation is violated sometimes arises when fitting the hydrogen Balmer lines (the Balmer problem). This is where lower order Balmer lines appear too weak, while higher order lines are too strong, resulting in a range of T_{eff} fitting different regions of the spectrum (cf. Latour et al. 2015). For this analysis the adopted value of T_{eff} was the mean obtained after fitting five Balmer lines individually. While $H\alpha$ is not well fit by our models, there is good agreement between the other four lines, so that T_{eff} , $\log g$, and helium fraction are obtained with confidence.

SFIT provides several algorithms designed to fit a model spectrum to the observed data. That used here is the Levenburg-Marquardt downhill simplex, which takes initial parameters and calculates the derivative of each with respect to χ_{red}^2 . The algorithm then takes a step downhill by a distance determined by the steepness of the slope, and repeats this until a minimum χ_{red}^2 is found. As the algorithm approaches a minimum, finer steps are taken to improve accuracy. Once T_{eff} , g , and n_{He} have been computed, abundances for each element or ion with atomic data available were fitted individually. Abundances for each element are measured separately for each spectral region observed, and then combined using a weighted mean. Errors given on the weighted mean are found by summing the reciprocal errors in quadrature.

The Levenburg-Marquardt algorithm provides standard errors in its analysis of any parameter and these are generally included. However, for many areas of the spectra where line blanketing is too severe and the spectrum rarely reaches the continuum, the automated process may not distinguish between spectral lines and an extremely low signal to noise ratio. It is therefore unable to accurately fit the abundances, and may fit a straight line through the middle of the spectral lines. In order to proceed, the fit was conducted by hand

and the abundance was manually adjusted until a best fit was identified. The errors were then determined by adjusting the abundance until the fit was judged to be unsatisfactory in a "χ-by-eye" method. Standard errors are given where available. The number of absorption lines of each element having a theoretical equivalent width $W_{\lambda} > 5\text{m\AA}$ that contribute to the fit in each spectral region is also recorded.

In order to represent the quantity of any given element in each star, we employ the following formula for chemical abundance of element i :

$$\log \epsilon_i = \log \frac{n_i}{\sum_i n_i} + c \quad (1)$$

where c is determined such that $\log \sum_i \mu_i \epsilon_i + c = \log \sum_i \mu_i \epsilon_{i\odot} + c' = 12.15$ and μ_i is the atomic mass of element i . Abundances relative to solar values as given by Asplund et al. (2005) are given in logarithmic form and denoted by the atomic symbol in square brackets (e.g. $[C] = \log(\epsilon_C/\epsilon_{C\odot})$).

3.1 Atomic data

The atomic data used in this analysis were compiled from several sources. We began with the database provided by Aggarwal et al. (2017). This was augmented to include data on Zn, Ga, Ge, Sr, and Ba from Rauch et al. (2015). Where duplicate entries were found, the latter source was preferred due to being specific to those elements. The resulting data were then merged with the Kurucz atomic database (Kurucz et al. 2016). Again, where duplicate entries were found, the latter were used.

We searched for Pb IV lines using theoretical oscillator strengths from Alonso-Medina et al. (2011). These data were extracted and merged into our atomic line database.

Because both stars have temperatures in the region of 40 000K, there are substantial fractions of highly ionised species. Due to the conditions that produce these ions being difficult to recreate, experimental oscillator strengths are frequently either poor or missing. Theoretical values exist for some ions, and were used for the heavier elements where no experimental data are available.

Despite gathering as much data as possible, both stars contain a large fraction of lines that we were unable to model. For example, when analysing the FUV region of PG 0909+276, a total of 806 lines, roughly 20% of an estimated 3,600 lines, were successfully used to extract abundances. Similarly, in the NUV, an estimated 2,400 lines are

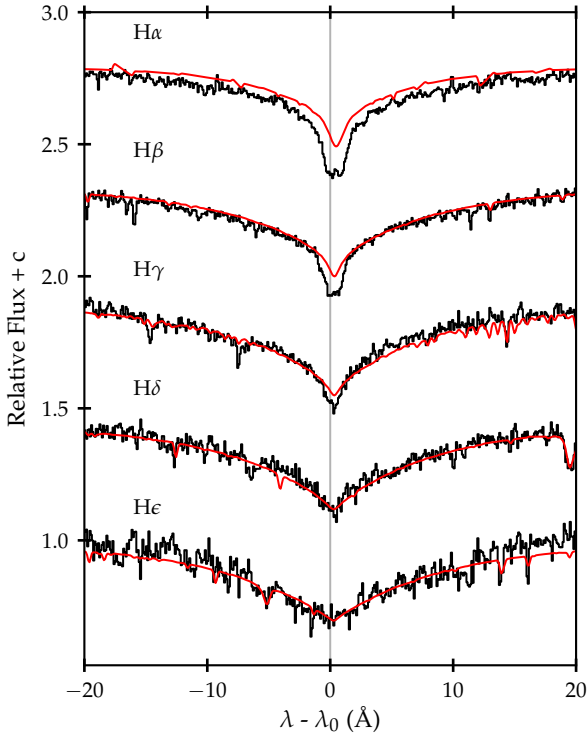


Figure 1. The Balmer lines of PG 0909+276, showing the difficulty in fitting the hydrogen line cores and wings simultaneously.

Star / Data	T_{eff}/K	$\log g/\text{cm s}^{-2}$	n_{He}	$E(B-V)$
PG 0909+276				
DSAZ	$37,290 \pm 640$	6.10 ± 0.20	0.126 ± 0.008	0.05
IUE	$37,160 \pm 220$	-	-	-
UVO 0512-08				
DSAZ	$36,670 \pm 1,430$	5.75 ± 0.16	0.159 ± 0.062	0.05
IUE	$36,670 \pm 260$	-	-	-

Table 2. Basic parameters derived for programme stars from high-resolution spectroscopy (STIS) and spectrophotometry (IUE).

detected, and of these, 936 (39%), were successfully identified and contributed to abundance measurements.

4 RESULTS: PG 0909+276

4.1 Basic Parameters

The three wavelength regions were treated independently. The optical region (3900Å- 6900Å) contains the majority of hydrogen and helium lines, which were used to fit the basic parameters: T_{eff} , g and H and He number fractions. Since these parameters are strongly correlated, they were fitted simultaneously. The best fit with formal errors is $T_{\text{eff}} = 37,290 \pm 640\text{K}$, $\log g/\text{cm s}^{-2} = 6.10 \pm 0.20$, and helium number fraction $n_{\text{He}} = 0.126 \pm 0.008$.

PG 0909+276 expressed the Balmer problem, shown in Fig. 1, with the H α line showing the largest deviation. With good agreement between the other four lines, we have confidence in the adopted parameters.

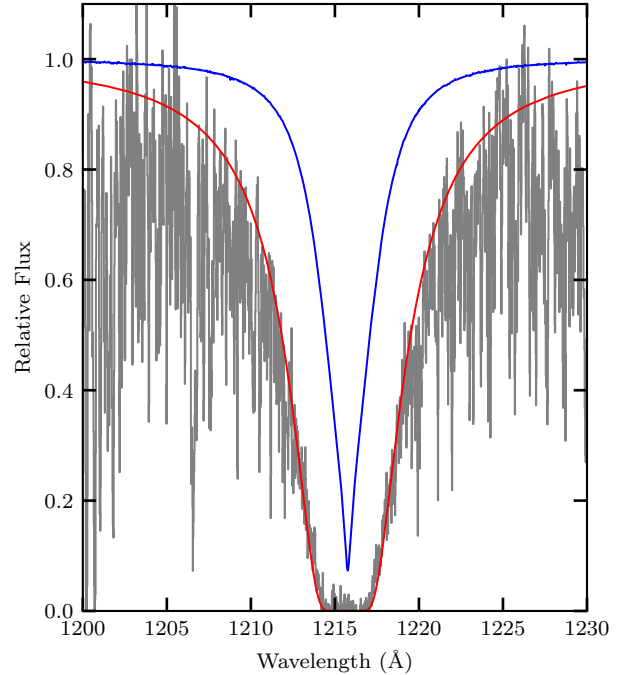


Figure 2. The FUV spectrum of PG 0909+276 in the region of Ly α (grey) is shown together with the theoretical photospheric profile assuming $n_{\text{He}} = 0.126$ (blue) and the theoretical interstellar profile for a hydrogen column density of $2.39 \times 10^{20} \text{cm}^{-2}$ (red).

The FUV Lyman α line could not be modelled by stellar absorption in either star. In both cases, the line is successfully modelled by including absorption due to interstellar hydrogen [Groenewegen & Lamers \(1989\)](#). This feature was best fit by a model with hydrogen column density of $2.39 \times 10^{20} \text{cm}^{-2}$ (Fig. 2)

We had difficulty fitting He II 1640.37Å. Unexpected structure in the core was poorly fitted when the line was modelled as a single line ([Schöning & Butler 1989](#)). He II 1640.37Å consists of a multiplet with seven fine-structure components. We improved the theoretical profile by treating all seven components individually, using their respective wavelengths and statistical weights from LS coupling. The result did not reproduce the observed structure, instead we observed a slightly weakened overall line strength (Fig 3). The observed structure is likely due to a combination of non-LTE processes and unidentified lines from other atomic species.

4.2 Non-Stellar Lines

Once the basic parameters had been determined, we identified as many non-stellar lines as possible. We checked Table 2 of [Morton \(1978\)](#) for known interstellar lines, and masked these from the data in subsequent analyses. The optical spectrum of PG 0909+276 also contained a number of strong neutral thorium lines. These presumably arise from contamination by the wavelength calibration lamp. They were iden-

Z	N	Mean	$\log \epsilon / \epsilon_{\odot}$	FUV	NUV	OP	NUV-FUV	OP-FUV	OP-NUV
H	0/0/5	11.70 ± 0.10	-0.30	–	–	11.70 ± 0.10	–	–	–
He	1/0/14	11.04 ± 0.12	0.11	11.05 ± 0.15	–	11.02 ± 0.18	–	-0.03 ± 0.23	–
C	30/12/32	8.68 ± 0.12	0.25	8.62 ± 0.18	8.78 ± 0.20	8.61 ± 0.30	0.16 ± 0.27	-0.01 ± 0.35	-0.17 ± 0.36
N	2/5/15	7.93 ± 0.13	0.10	7.80 ± 0.48	7.77 ± 0.25	8.02 ± 0.17	-0.03 ± 0.54	0.22 ± 0.51	0.25 ± 0.30
Si	9/0/0	5.95 ± 0.20	-1.56	5.95 ± 0.20	–	–	–	–	–
S	36/36/8	8.20 ± 0.14	1.08	8.59 ± 0.25	8.50 ± 0.30	7.81 ± 0.20	-0.09 ± 0.39	-0.78 ± 0.32	-0.69 ± 0.36
Ar	34/35/2	8.36 ± 0.11	1.96	8.29 ± 0.28	8.41 ± 0.15	8.30 ± 0.20	0.12 ± 0.32	0.01 ± 0.34	-0.11 ± 0.25
Ca	25/30/15	8.20 ± 0.10	1.86	8.30 ± 0.27	8.37 ± 0.13	7.73 ± 0.20	0.07 ± 0.30	-0.57 ± 0.34	-0.64 ± 0.24
Sc	9/28/39	7.66 ± 0.12	4.51	7.64 ± 0.25	7.30 ± 0.30	7.75 ± 0.15	-0.34 ± 0.39	0.11 ± 0.29	0.45 ± 0.34
Ti	0/14/24	7.69 ± 0.11	2.74	–	7.50 ± 0.23	7.75 ± 0.13	–	–	0.25 ± 0.26
V	6/58/5	7.32 ± 0.13	3.39	6.30 ± 0.25	7.49 ± 0.18	8.00 ± 0.25	1.19 ± 0.31	1.70 ± 0.35	0.51 ± 0.31
Cr	79/150/0	7.59 ± 0.17	1.95	7.45 ± 0.23	7.75 ± 0.25	–	0.30 ± 0.34	–	–
Mn	0/46/0	7.02 ± 0.15	1.59	–	7.02 ± 0.15	–	–	–	–
Fe	67/0/0	7.10 ± 0.20	-0.40	7.10 ± 0.20	–	–	–	–	–
Co	160/328/0	7.97 ± 0.17	2.98	7.73 ± 0.23	8.25 ± 0.25	–	0.52 ± 0.34	–	–
Ni	277/186/0	7.88 ± 0.14	1.66	7.85 ± 0.15	8.00 ± 0.33	–	0.15 ± 0.36	–	–
Cu	56/7/0	7.18 ± 0.15	2.99	6.90 ± 0.28	7.30 ± 0.18	–	0.40 ± 0.33	–	–
Zn	14/0/0	6.50 ± 0.15	1.94	6.50 ± 0.15	–	–	–	–	–
Ga	14/0/0	4.90 ± 0.15	1.86	4.90 ± 0.15	–	–	–	–	–
Ge	2/0/0	6.80 ± 0.20	3.15	6.80 ± 0.20	–	–	–	–	–
Sn	1/0/0	3.60 ± 0.20	1.56	3.60 ± 0.20	–	–	–	–	–
Pb	1/1/0	4.29 ± 0.12	2.54	4.40 ± 0.15	4.10 ± 0.20	–	-0.30 ± 0.25	–	–

Table 3. Abundance results for PG 0909+276 in the three spectral regions, and the mean weighted by the square of the errors. The differences, where available, between abundance measurements are shown. The standard deviation is presented here not as a statistical tool, but rather as a loose indicator due to only using two or three data.

4403.42	4403.71	4485.71	4504.63	4435.25	4440.35
4485.71	4488.68	4504.26	4916.12	4948.97	4964.12
4968.75	4976.59	4992.13	5070.78	5106.67	5219.11
5243.74	5352.99	5399.17			

Table 4. Wavelengths of lines in the spectrum of PG 0909+276 attributed to non-stellar thorium, and excluded from fits.

tified and masked in the same fashion as interstellar lines. A list is included in Table 4. In our analysis of UVO 0512–08, we used the same procedure to mask interstellar features, and did not detect neutral thorium lines.

4.3 C, N, O, Si, Ca, Fe

As the model atmosphere requires some metal abundances as an input, these were the first to be measured. The final measured values for all elements are contained in Table 3 with errors, including the weighted mean.

Carbon was found to have a mean abundance $\log \epsilon_{\text{C}} = 8.68 \pm 0.12$ over the three regions, with very good agreement. A good number of lines were present in all three regions. The nitrogen abundance is well-constrained across all three data sets with a mean value $\log \epsilon_{\text{N}} = 7.93 \pm 0.13$. We were unable to find an abundance for oxygen, as there were no observed lines in the spectrum. We found a limit $\log \epsilon_{\text{O}} \lesssim 6.00$ above which O IV 1343.51Å should be observable. The carbon and nitrogen abundances are close to solar, in agreement with [Edelmann \(2003\)](#).

Obtaining an abundance for iron is limited by the lack of clear iron lines in the optical and NUV. In both regions we constrain $\log \epsilon_{\text{Fe}} \lesssim 7.50$; at this abundance unobserved lines begin to exceed the noise. The FUV contains several iron lines; and these give an abundance $\log \epsilon_{\text{Fe}} = 7.10 \pm 0.20$.

This comes from a sample of lines of which roughly half are blended with another element. Several strong unobserved lines begin to appear above abundances of $\log \epsilon_{\text{Fe}} = 7.30$, which we adopt as the upper limit.

Silicon is poorly represented with only 9 lines detected throughout the whole spectrum, all in the FUV. These lines are in good agreement with each other and give $\log \epsilon_{\text{Si}} = 5.95 \pm 0.20$. Contrary to C, N and O, the silicon abundance is substantially lower than solar at $[\text{Si}] = -1.560 \pm 0.200$.

Calcium shows 70 lines across the spectra. As the FUV and NUV abundances agree to within errors and the optical abundance does not, we combined the UV measurements to obtain a mean abundance $\log \epsilon_{\text{Ca}} = 8.55 \pm 0.19$, compared to $\log \epsilon_{\text{Ca}} = 7.73 \pm 0.20$ in the optical. This gives a discrepancy of 0.82 ± 0.28 between UV and optical, the implications of which are discussed in section 6

4.4 Inconsistent Abundance Measurements

Table 3 shows the differences between observed abundances for elements measured in more than one region. While many elements were either seen in only one region, or had abundances that were in agreement, we observed a 2σ discrepancy in three elements: S, Ca, and V.

We observed substantial depletion in the optical relative to the UV in both sulphur and calcium. However, we observed agreement across the UV in both. Thus, we take the mean of the FUV and NUV as one value and the optical as another value. For sulphur, we then have a UV abundance of $\log \epsilon_{\text{S}} = 8.55 \pm 0.19$. We calculated a discrepancy between the optical and UV of -0.74 ± 0.27 . Similarly, calcium has a UV abundance of $\log \epsilon_{\text{Ca}} = 8.35 \pm 0.12$. We also find a mean depletion in the optical of 0.63 ± 0.23 .

Vanadium was observed to have a significant disagreement between two regions, with differences of 1.19 ± 0.31

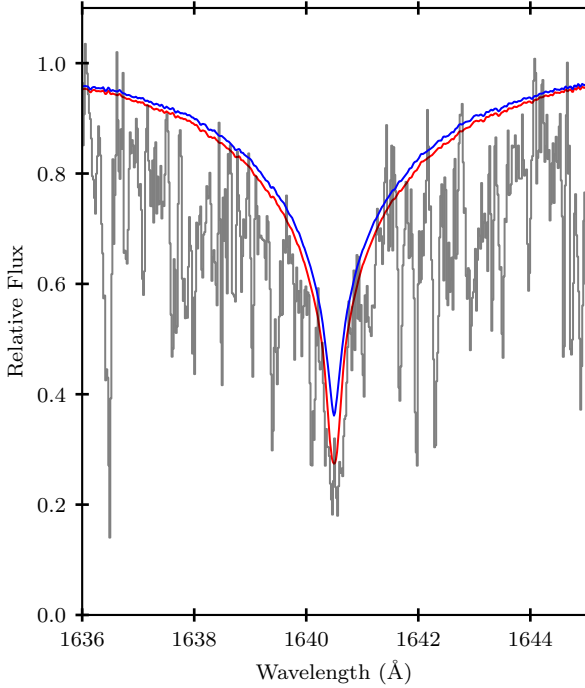


Figure 3. The observed spectrum of PG 0909+276 around the He II 1640.37Å line (grey). The theoretical line is modelled as a singlet (red) and including fine structure (blue).

between the NUV and FUV, and 1.70 ± 0.35 between the optical and FUV.

4.5 Other Elements

We detected two lead lines, at 1313.10Å and 1755.00Å which were modelled with atomic data from [Alonso-Medina et al. \(2011\)](#). From them, we infer that PG 0909+276 is rich in lead with an abundance of $\log \epsilon_{\text{Pb}} = 4.29 \pm 0.12$, or a number fraction of order 100 times solar.

We observed a line at 2335.26Å which could be attributed to Ba II and from which we would measure $\log \epsilon_{\text{Ba}} = 8.75 \pm 0.15$. We searched other regions of spectrum for barium lines (e.g. around 4130.65Å, 4554.03Å, and 4934.08Å), without success. Whilst a barium abundance of 8.75 is consistent with the optical lines not being seen, it represents an overabundance of > 6 dex and relies on a single line. We have therefore not shown barium in any of the summary tables (e.g. Table 3).

We probed for Ga, Ge, and Sn, as significant enrichments were observed previously by [O’Toole & Heber \(2006\)](#) in their analysis. We observed PG 0909+276 to have 14 gallium lines in the FUV consistent with an abundance $\log \epsilon_{\text{Ga}} = 4.90 \pm 0.15$. Similar to the stars studied by [O’Toole & Heber \(2006\)](#), PG 0909+276 is enriched by 1.86 ± 0.17 dex relative to a solar abundance of 3.04 ± 0.09 .

We observed the strong resonance Sn III 1251.39Å line. Unlike the previous stars, it does not occur as a blend. This line is very sensitive to abundance changes, and we were able

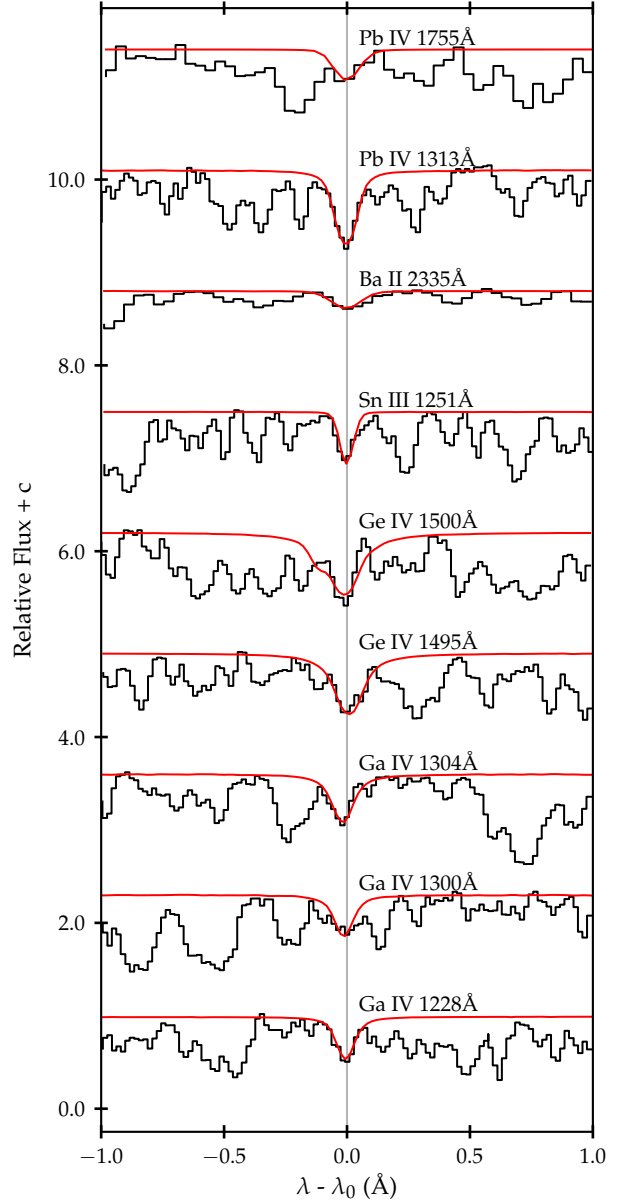


Figure 4. Line profiles of barium, lead, tin, gallium, and germanium lines for PG 0909+276, showing STIS spectrum (black histogram) and best-fit model (red).

to fit it to a model of $\log \epsilon_{\text{Sn}} = 3.60 \pm 0.20$. This is a relatively mild enrichment, only 1.46 dex relative to solar. The fit to this Sn III line, along with the Ga, Ge, Ba, and Pb lines from PG 0909+276 are shown in figure 4.

We noted two spectral lines at wavelengths [O’Toole & Heber \(2006\)](#) identified to be germanium, 1494.89Å and 1500.61Å. To match the line depths, we required an abundance of $\log \epsilon_{\text{Ge}} = 6.80 \pm 0.25$. Although extremely enriched (3.15 dex), similar levels have been found in other chemically peculiar sdB stars ([Naslim et al. 2011, 2013](#)). We checked NIST for alternative candidate lines without success.

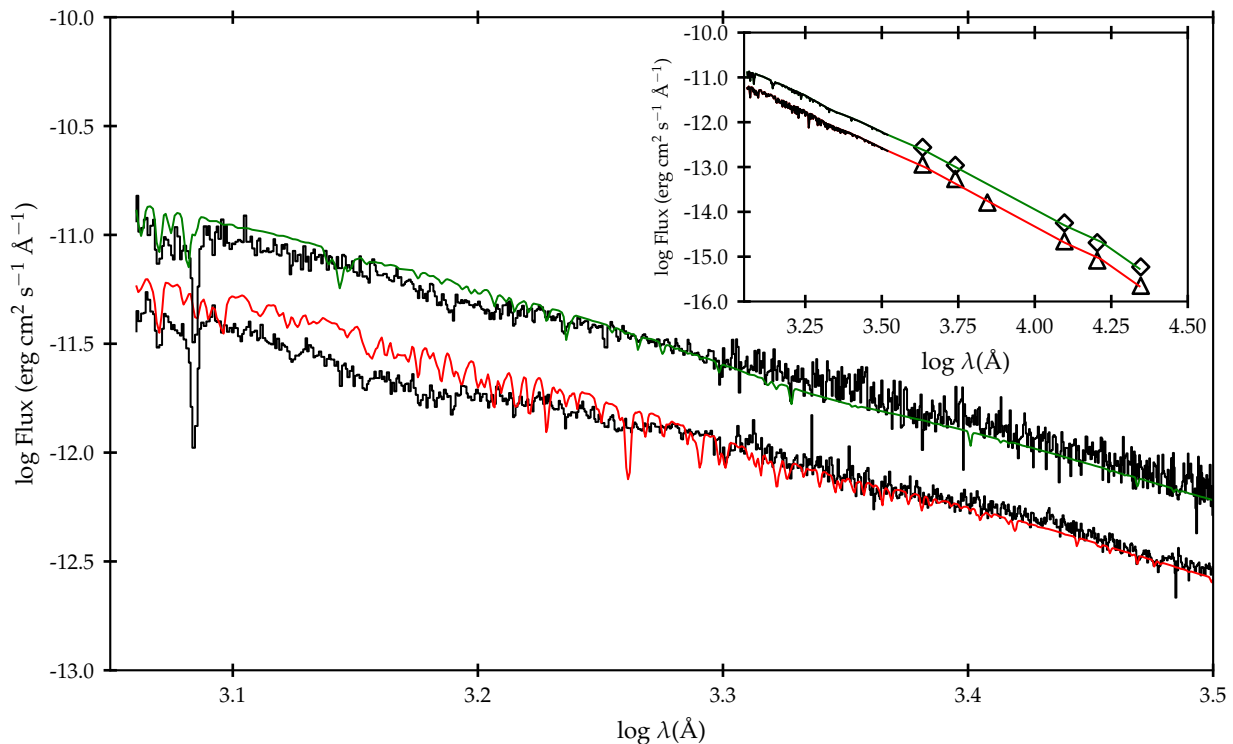


Figure 5. The IUE low-resolution spectrophotometry for UVO 0512–08 (upper black line) and PG 0909+276 (lower black line). The lower, red line is for a model with $T_{\text{eff}} = 37,160\text{K}$, and the green line is for a model with a $T_{\text{eff}} = 36,670\text{K}$. The inset compares models with broad-band photometry of PG 0909+276 in B, V, R, J, H, and K (Høg et al. 2000; Zacharias et al. 2009; Cutri et al. 2003) (triangles) and UVO 0512–08 in B, V, J, H, and K (Høg et al. 2000; Cutri et al. 2003) (diamonds).

4.6 IUE Data

We compared the output flux of our final models with low-resolution IUE and optical and near infra-red photometry. Due to the degeneracy between T_{eff} and $E(B-V)$, we fix $E(B-V)$ at the hydrogen column density matching the Lyman α line. Figure 5 shows that for wavelengths $3.3 < \log \lambda < 3.5$, the models match observation quite well, but the regions observed with STIS ($3.0 < \log \lambda < 3.3$) are more poorly fitted. Our best fit to the IUE data was for a model with $T_{\text{eff}} = 37,290 \pm 220$, $E(B-V) = 0.05$, and angular radius $\theta = 8.78 \pm 0.01 \times 10^{-12}$ radians. These solutions also match the B, V, R, J, H, and K broad-band photometry well (Drilling et al. 2013; Høg et al. 2000; Zacharias et al. 2009; Cutri et al. 2003).

As already indicated, there is substantial line opacity missing from the models at FUV wavelengths. We investigated models in which (a) all metals were increased by factors of 0.5(0.5)3.0 dex and (b) individual metal abundances were matched to those obtained by fine analysis, where iron is not significantly enhanced. Both tests assumed an homogeneous atmosphere. In case (a), we found substantial line blocking in the FUV region, but much of this appeared to come from a number of very strong lines which are not resolved in the IUE spectrum and for which there is no evidence in the HST/STI spectrum. In case (b), we found negligible difference compared with the models shown on Fig. 5.

5 RESULTS: UVO 0512–08

5.1 Basic Parameters

We performed the initial analysis for UVO 0512–08 identically to that for PG 0909+276. First, the optical H and He lines were fitted using a grid of atmosphere models in T_{eff} , $\log g$ and helium fraction. This yielded values of $36,670 \pm 1,430\text{K}$, 5.75 ± 0.16 , and 0.159 ± 0.062 respectively. Figure 6 shows the Balmer lines present in the optical region where it can be seen that the Balmer problem is more severe in UVO 0512–08 than in PG 0909+276. In particular, He and H α lines are not well fitted. This is reflected in the larger errors attached to the T_{eff} measurement.

Interstellar lines were removed in a similar fashion to PG 0909+276. We noted the same problem with modelling the 1640.37Å He II line, and were similarly unable to reproduce the profile accurately.

The Lyman α line was also fitted to interstellar absorption, where we found a good fit to a hydrogen column density of $2.39 \times 10^{20} \text{cm}^2$. Figure 7 shows the difference between the best-fit stellar and interstellar models.

Measurements of individual elemental abundances for UVO 0512–08 were obtained (as for PG 0909+276) by optimizing the theoretical line spectrum to the observed spectra. Results for the three wavelength regions are given in Table 5.

Z	N	Mean	$\log \epsilon / \epsilon_{\odot}$	FUV	NUV	OP	NUV-FUV	OP-FUV	OP-NUV
H	0/0/5	11.80 ± 0.04	-0.20	-	-	11.80 ± 0.04	-	-	-
He	1/0/14	11.16 ± 0.16	0.23	11.20 ± 0.29	-	11.14 ± 0.19	-	-0.06 ± 0.35	-
C	22/40/49	8.54 ± 0.10	0.11	8.39 ± 0.13	9.03 ± 0.22	8.47 ± 0.28	0.64 ± 0.26	0.08 ± 0.31	-0.56 ± 0.36
N	7/13/13	7.67 ± 0.16	-0.16	7.91 ± 0.38	7.68 ± 0.22	7.48 ± 0.31	-0.23 ± 0.44	-0.43 ± 0.49	-0.20 ± 0.38
Ne	0/13/9	8.32 ± 0.25	0.39	-	8.90 ± 0.53	8.15 ± 0.29	-	-	-0.75 ± 0.60
Mg	0/9/0	8.52 ± 0.73	0.92	-	8.52 ± 0.73	-	-	-	-
Al	1/0/0	5.50 ± 0.58	-0.95	5.50 ± 0.58	-	-	-	-	-
Si	3/0/0	4.91 ± 0.40	-2.60	4.91 ± 0.40	-	-	-	-	-
S	19/24/26	7.62 ± 0.18	0.50	7.19 ± 0.27	7.72 ± 0.42	8.14 ± 0.31	0.53 ± 0.50	0.95 ± 0.41	0.42 ± 0.52
Ar	55/67/14	8.39 ± 0.13	1.99	8.31 ± 0.18	8.57 ± 0.23	8.32 ± 0.30	0.26 ± 0.29	0.01 ± 0.35	-0.25 ± 0.38
Ca	59/82/34	8.51 ± 0.14	2.17	8.77 ± 0.20	8.55 ± 0.26	7.88 ± 0.30	-0.22 ± 0.33	-0.89 ± 0.36	-0.67 ± 0.40
Sc	2/2/7	7.20 ± 0.23	4.05	6.91 ± 0.39	6.68 ± 1.36	7.39 ± 0.30	-0.23 ± 1.41	0.48 ± 0.49	0.71 ± 1.39
Ti	17/34/9	7.99 ± 0.19	3.04	7.76 ± 0.45	7.76 ± 0.30	8.32 ± 0.30	0.00 ± 0.54	0.56 ± 0.54	0.56 ± 0.42
V	40/19/0	6.84 ± 0.17	2.91	6.72 ± 0.20	7.14 ± 0.32	-	0.42 ± 0.38	-	-
Cr	331/317/0	8.67 ± 0.12	3.03	8.20 ± 0.70	8.68 ± 0.12	-	0.48 ± 0.71	-	-
Mn	53/13/0	7.50 ± 0.24	2.07	7.52 ± 0.34	7.48 ± 0.33	-	-0.04 ± 0.47	-	-
Fe	348/342/15	8.53 ± 0.04	1.03	8.49 ± 0.05	8.70 ± 0.09	8.00 ± 0.29	0.21 ± 0.10	-0.49 ± 0.29	-0.70 ± 0.30
Co	221/354/0	8.45 ± 0.09	3.46	7.60 ± 0.28	8.56 ± 0.10	-	0.96 ± 0.30	-	-
Ni	119/117/0	7.25 ± 0.08	1.03	7.00 ± 0.09	8.26 ± 0.18	-	1.26 ± 0.20	-	-
Cu	53/6/0	6.74 ± 0.12	2.55	6.35 ± 0.15	7.30 ± 0.18	-	0.95 ± 0.23	-	-
Zn	101/4/0	7.25 ± 0.16	2.69	7.25 ± 0.16	7.30 ± 2.23	-	0.05 ± 2.24	-	-
Ga	8/0/0	4.65 ± 0.15	1.61	4.65 ± 0.15	-	-	-	-	-
Ge	2/0/0	6.60 ± 0.20	2.95	6.60 ± 0.20	-	-	-	-	-
Sn	1/0/0	4.40 ± 0.20	2.36	4.40 ± 0.20	-	-	-	-	-
Pb	1/1/0	4.22 ± 0.13	2.47	4.95 ± 0.30	4.04 ± 0.15	-	-0.91 ± 0.34	-	-

Table 5. Abundance results for UVO 0512–08 in the three spectral regions, and the mean weighted by the square of the errors. The differences, where available, between abundance measurements are shown. The standard deviation is presented here not as a statistical tool, but rather as a loose indicator due to only using two or three data.

5.2 C, N, O, Si, Ca, Fe

We observed agreement in the carbon abundance between the FUV and optical about $\log \epsilon_{\text{C}} = 8.48 \pm 0.07$; in the NUV, we found $\log \epsilon_{\text{C}} = 9.03 \pm 0.22$, a discrepancy of 0.55 ± 0.25 dex.

We found only 19 nitrogen lines in the FUV and NUV, many of which were strong. We found a value close to solar in all three regions, with a mean of $[\text{N}] = -0.16$.

We did not observe any oxygen lines in any regions of the spectrum. In order for no lines with equivalent widths $>5\text{m}\text{\AA}$ to be seen, the abundance of oxygen in the star must be less than $\log \epsilon_{\text{O}} \sim 5.50$, or $[\text{O}] < -3.19$. Normal sdBs typically have $[\text{O}] \approx -1$, making this a very oxygen-deficient subdwarf.

For silicon, we only detected 3 strong lines in the FUV, giving an abundance $[\text{Si}] = -2.60$. In the case of calcium, the FUV and NUV abundances agreed well, yielding a weighted mean of $\log \epsilon_{\text{Ca}} = 8.51 \pm 0.14$. The optical spectrum gave $\log \epsilon_{\text{Ca}} = 7.88 \pm 0.30$, or a difference of -0.63 ± 0.33 .

We observed several hundred iron lines in the UV spectra of UVO 0512–08, unlike PG 0909+276 which expressed very few iron features. Agreement was observed between FUV and NUV spectra. 5 Weak Fe lines in the optical between 4318.20\AA and 4310.80\AA required an abundance lower by 0.57 ± 0.21 . Fig. 8 demonstrates how lowering the optical abundance improves the fit to these lines.

5.3 Inconsistent Abundance Measurements

For UVO 0512–08, we detected abundance discrepancies exceeding 2σ between spectral regions in eight elements. Carbon, calcium and iron were discussed above. We also ob-

served disagreement in sulphur, cobalt, nickel, copper and lead.

Sulphur is well constrained in all three wavelength regions. FUV and NUV agree well, but the optical – FUV difference is 0.95 ± 0.41 .

Cobalt lines were seen in both FUV and NUV in very large numbers, with a large disagreement in abundance which is emphasized by the small error on the NUV measurement of $\log \epsilon_{\text{Co}} = 8.56 \pm 0.10$. The NUV abundance is larger than the FUV value by 0.96 ± 0.30 dex.

We detected strongly differing quantities of nickel in the two UV regions, which both contain over 100 lines. The NUV abundance is larger by 1.26 ± 0.20 dex.

Copper shows an NUV abundance larger than the the FUV by 0.95 ± 0.23 dex. While more lines were detected in the FUV, they often occur in busier segments of the spectrum, requiring them to be fitted by hand.

The FUV and NUV titanium abundances are similar, but lower than the optical by 0.56 ± 0.54 and 0.56 ± 0.42 dex, respectively.

Finally, we found a disagreement between abundances given by the two lead lines (1755.00\AA and 1313.10\AA) of -0.91 ± 0.34 dex. The average of the two abundances gives $\log \epsilon_{\text{Pb}} = 4.22 \pm 0.13$. The model fits are shown in figure 9.

5.4 Other Elements

We conducted a search for features due elements with $Z > 30$ for which atomic data are available. We found no traces of the majority, germanium, arsenic, strontium, yttrium, tin, and barium.

In the cases of magnesium, aluminium and silicon, we

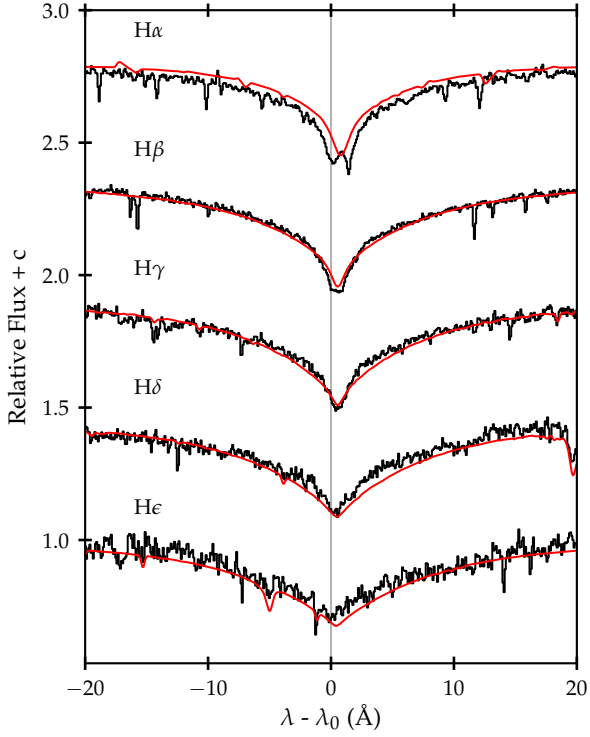


Figure 6. The observed Balmer lines (black) and models (red) in UVO 0512-08.

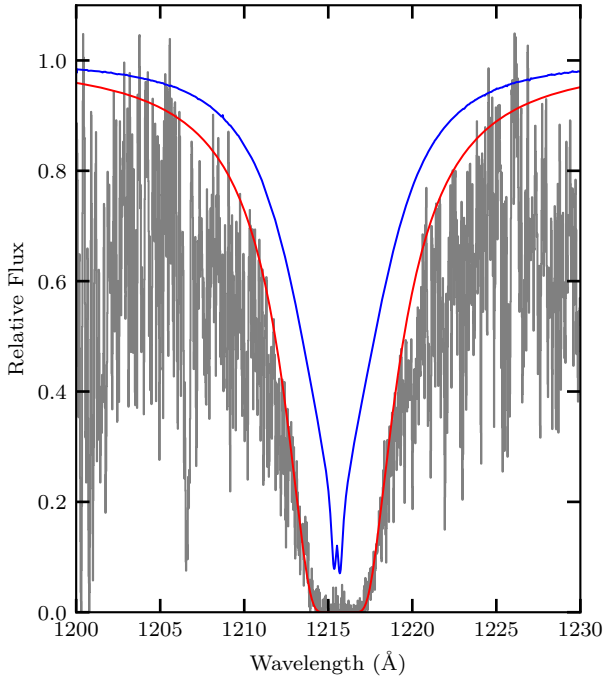


Figure 7. The FUV spectrum of UVO 0512-08 in the region of Ly α (black) together with the theoretical photospheric profile assuming $n_{\text{He}} = 0.159$ (blue) and the theoretical interstellar profile assuming a hydrogen column density of $2.39 \times 10^{20} \text{ cm}^2$

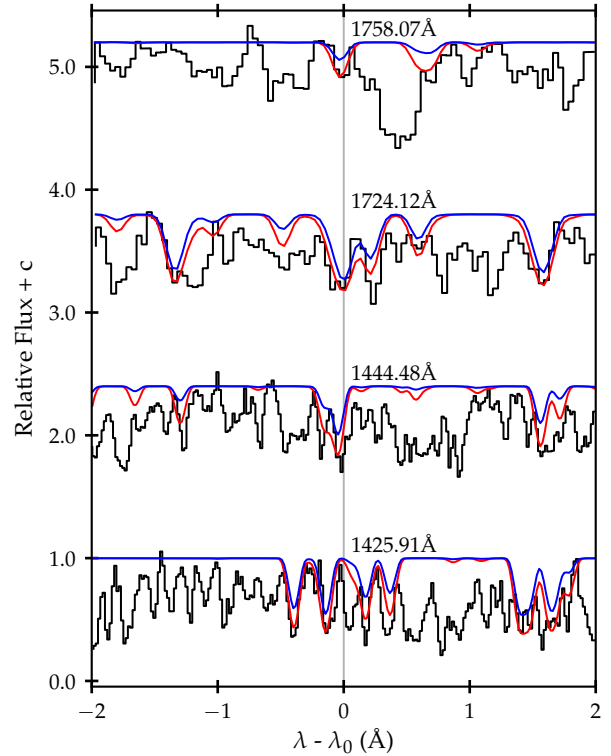
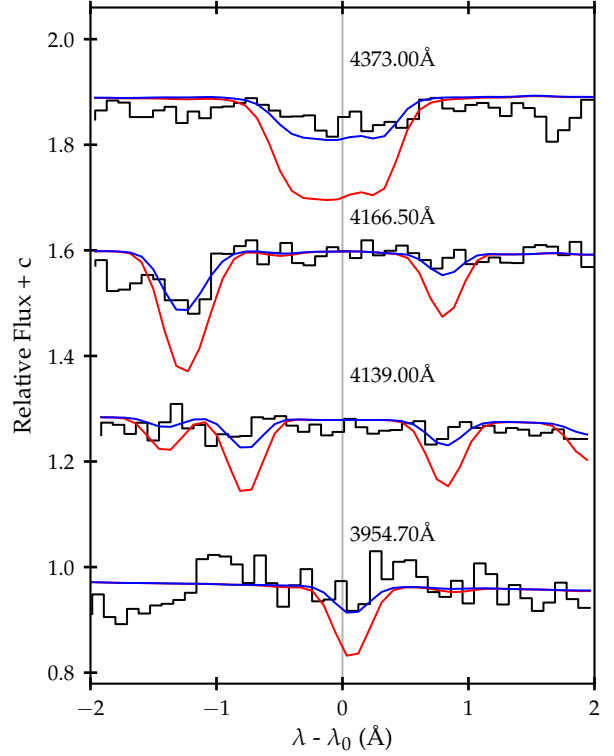


Figure 8. Upper: Models of FeIII lines in the optical region of UVO 0512-08 (black) with $\log \epsilon_{\text{Fe}} = 8.0$ (blue) and 8.7 (red). The labels above each observation denotes λ_0 for that section. Lower: The above plot is duplicated for the UV regions. These plots are separated due to differing scales.

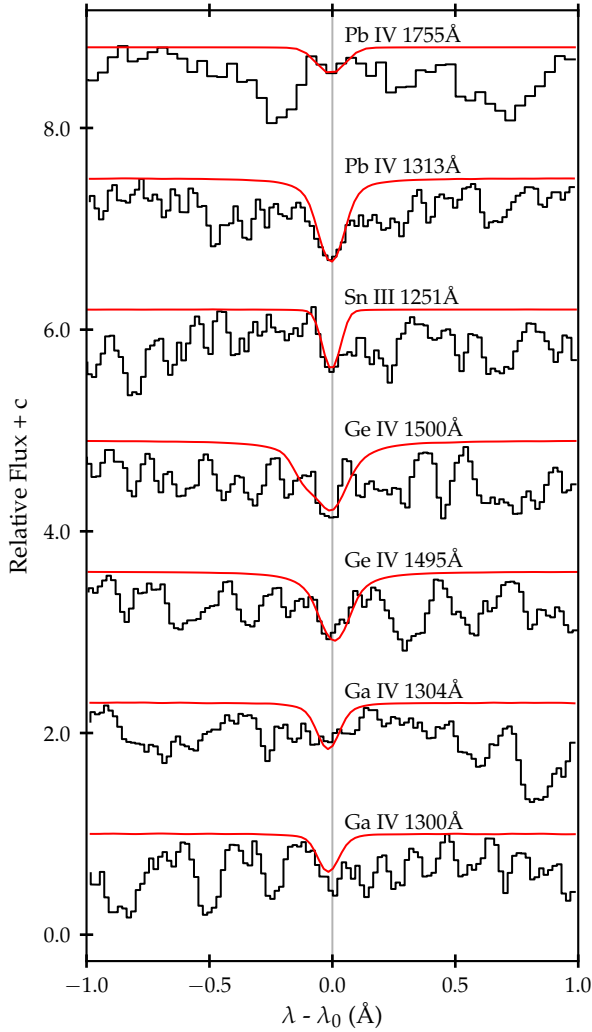


Figure 9. A selection of UVO 0512-08 model Ga IV, GeIV, SnIII, and Pb IV lines (red). The STIS observations are shown in black.

detected spectral lines in only one region. We observed magnesium to be enriched relative to other sdBs with $[Mg] = 0.92$, in contrast to the sub-solar values of all other sdBs in figure 10. Aluminium is consistent with previous measurements of sdBs.

While we did not observe any of the germanium lines seen in PG 0909+276, we detected eight gallium lines in the FUV, which gave us an abundance of $\log \epsilon_{Ga} = 4.65 \pm 0.15$ (or $[Ga] = 1.61 \pm 0.16$). The Sn II 1251.39Å line seen in PG 0909+276 and by O’Toole & Heber (2006) was also seen in this star, and was well modelled by an enrichment of $[Sn] = 2.36$. This is shown in figure 9

For a further six elements nitrogen, argon, scandium, chromium, manganese, and zinc, we detected no significant discrepancies across the wavelength regions in which they were observed, and no significant departures from the typical abundances of sdB stars.

5.5 IUE Data

As in PG 0909+276, we fixed $E(B-V)$ to match the column density of hydrogen found with the Lyman α line. Our fit to the IUE spectrophotometry for UVO 0512-08 gives $T_{\text{eff}} = 36,670 \pm 260\text{K}$, $E(B-V) = 0.05$, and $\theta = 1.35 \pm 0.01 \times 10^{-11}$ radians (Fig. 5). T_{eff} is consistent with the optical observations. The observed Ly α line can be seen at $\log \lambda = 3.085$ and, as in the STIS spectroscopy, is dominated by interstellar hydrogen (cf. Fig. 7).

6 DISCUSSION

Figure 10 shows the surface chemical abundance data for several metal-rich subdwarfs from previous analyses, as well as for the stars studied in this paper, as measured relative to the standard solar surface composition (Asplund et al. 2009). It shows the general upwards trend for heavier metals to be more enriched. The linked circles showing the abundance ranges for ‘normal’ hot subdwarfs illustrate this.

In both PG 0909+276 and UVO 0512-08, all observed elements with $Z \geq 16$ are enriched compared to solar. Elements with $Z < 16$ are either roughly solar or, in the case of silicon, strongly subsolar. Whilst most hot subdwarfs show roughly solar surface nitrogen, the majority are carbon poor. In contrast, PG 0909+276 and UVO 0512-08 are carbon rich relative to other hot subdwarfs.

Although the majority of both normal sdB stars and peculiar subdwarfs have an iron abundance close to solar, UVO 0512-08 is detectably iron-rich, with $[Fe] = 1.070 \pm 0.040$. We postulate that this is either due to iron stratification in the atmosphere or to the progenitor composition.

Figure 10 shows the position in T_{eff} and $\log g/\text{cm s}^{-2}$ of both stars in this analysis, alongside other peculiar subdwarfs and the populations of known H-rich and He-rich subdwarfs. We can see that both stars sit near the zero-age He main sequence, similar to other peculiar sdB stars.

We detected significant inconsistencies in several elements in each star. Tables 3 and 5 summarise these discrepancies, and a regression fit was performed on these data. We found no statistically significant trends in the discrepancies of PG 0909+276 or UVO 0512-08. In the absence of any evidence for stratification in either star, we conclude that it is likely that both stars are intrinsically enriched with heavy elements to a degree rarely seen in hot subdwarfs. The question of why this subcategory of sdO/B stars is so rich in heavy metals remains open, and requires further thought. We have not ruled out the possibility of stratification by radiative levitation, but if this is to be observed, more sensitive methods are needed.

7 CONCLUSION

We have carried out spectroscopic fine analyses of two helium-enriched hot subdwarfs, PG 0909+276 and UVO 0512-08. These are based on new ultraviolet spectra obtained with the *Hubble Space Telescope*, and a re-analysis of the optical spectra obtained by Edelmann (2003). From the latter, we have remeasured T_{eff} , $\log g/\text{cm s}^{-2}$, and n_{H} and n_{He} , as well as the abundances of C, N, Ne, S, Ar, Ca, Sc, Ti, V and Fe. The new ultraviolet observations allowed us

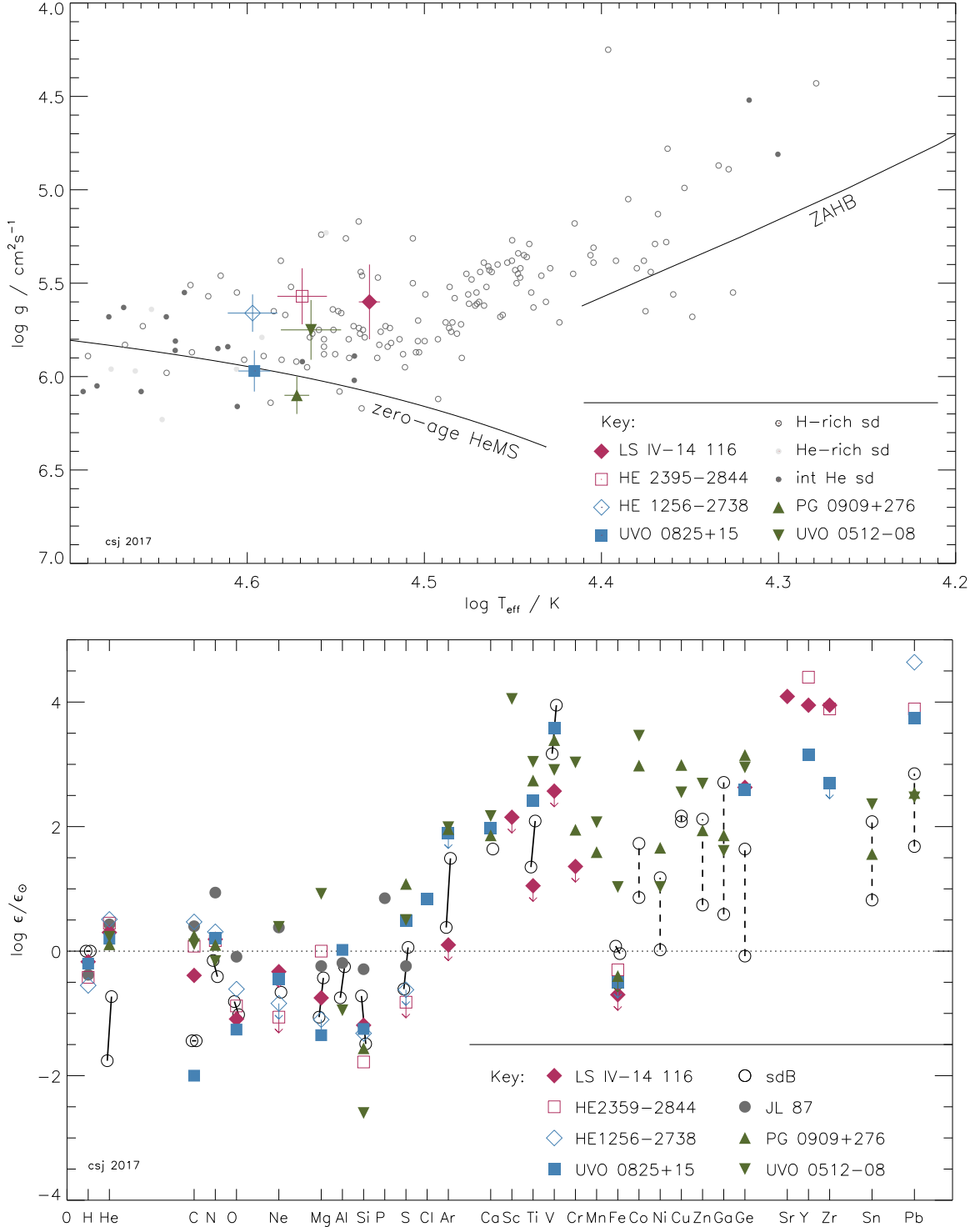


Figure 10. Top: The distribution of chemically-peculiar, helium-rich and normal hot subdwarfs with effective temperature and surface gravity. The solid line shows representative positions for the theoretical zero-age helium main-sequence (HeMS: $Z = 0.02$) and zero-age horizontal branch (ZAHB). The observed data are from this work, Naslim et al. (2011, 2013); Jeffery et al. (2017) and Németh et al. (2012). **Bottom:** Surface abundances of super metal-rich hot subdwarfs, including the pulsating stars LS IV-14° 116 and UVO 0825+15, and the two stars considered in this paper; UVO 0512-08 and PG 0909+276. Abundances are shown relative to solar values (dotted line). Mean abundances and ranges for the helium-rich subdwarf JL 87 (Ahmad et al. 2007) and for normal subdwarfs are also shown. The latter are shown by connected open circles as (i) $Z \leq 26$ (solid lines): the average abundances for cool and warm sdBs (Geier 2013) and (ii) $Z \geq 27$ (broken lines): the range of abundances measured for five normal sdBs from UV spectroscopy (O’Toole & Heber 2006).

Table 6. Elemental abundances for PG 0909+276, UVO 0512–08, and related stars in the form $\log \epsilon_i = \log n_i + c$ (see text). Measurement errors are shown in parenthesis. The absence of a reported measurement is indicated by “–”.

Star	H	He	C	N	O	Ne	Mg	Al	Si	S	Cl	Ar
PG 0909+276 ^a	11.70(10)	11.04(12)	8.68(12)	7.94(13)	–	–	–	–	5.95(20)	8.20(14)	–	8.36(11)
PG 0909+276 ^{1,2}		11.15(10)	8.63(35)	8.00(23)	< 6.00	< 7.87	–	< 6.25	5.80(10)	8.26(53)	–	8.68(15)
UVO 0512–08 ^a	11.80(04)	11.16(16)	8.54(10)	7.67(16)	–	8.32(25)	8.52(73)	5.50(58)	4.91(40)	7.62(18)	–	8.39(13)
UVO 0512–08 ^{1,2}		11.23(10)	8.59(20)	7.94(21)	< 5.50	–	–	< 6.25	5.76	8.14(49)	–	9.90
UVO 0825+15 ³	11.8	11.2	< 6.5	8.04(24)	7.43(07)	7.48(25)	6.25(11)	6.47(07)	6.26(21)	7.61(18)	6.34(11)	< 8.3
LS IV–14°116 ⁴	11.83	11.23(05)	8.04(22)	8.02(20)	7.60(17)	< 7.6	6.85(10)	–	6.32(12)	–	–	–
HE 1256–2738 ⁵	11.45	11.44	8.90(54)	8.14(62)	8.08(10)	< 7.1	< 6.5	–	6.19(10)	< 6.5	–	–
HE 2359–2844 ⁵	11.58	11.38	8.51(29)	8.00(57)	7.81(16)	< 6.9	7.6(1)	–	5.73(13)	< 6.3	–	–
JL 87 ⁶	11.62(07)	11.26(18)	8.83(04)	8.77(23)	8.60(23)	8.31(57)	7.36(33)	–	7.22(27)	6.88(1.42)	–	–
cool sdB ^{2,b}		9.24(54)	6.99(47)	7.68(41)	7.88(26)	–	6.54(26)	5.70(18)	6.79(37)	6.51(21)	–	6.78(21)
warm sdB ^{2,c}		10.15(76)	7.73(70)	7.42(27)	7.67(51)	7.27(67)	7.17(29)	6.2	6.02(55)	7.18(56)	–	7.89(17)
Feige 66 ⁷		10.4	6.79(30)	7.65(15)	–	–	–	< 3.5	< 2.0	7.69(46)	–	7.86(24)
Sun ⁸	12.00	10.93	8.43	7.83	8.69	7.93	7.60	6.45	7.51	7.12	5.50	6.40

Star	Ca	Ti	V	Cr	Fe	Co	Ni	Cu	Ga	Ge	Sn	Pb
PG 0909+276 ^a	8.20(10)	7.69(13)	7.32(13)	7.59(17)	7.10(20)	7.97(17)	7.88(14)	7.18(15)	4.90(15)	6.80(20)	3.60(20)	4.29(12)
PG 0909+276 ^{1,2}	7.81(35)	7.97(20)	8.10(26)	–	< 7.87	–	–	–	–	–	–	–
UVO 0512–08 ^a	8.51(14)	7.99(19)	6.84(17)	8.67(12)	8.53(04)	8.45(09)	7.25(08)	6.74(12)	4.65(15)	6.60(20)	4.40(20)	4.22(13)
UVO 0512–08 ^{1,2}	8.10(24)	8.06(33)	7.36(22)	–	< 7.81	–	–	–	–	–	–	–
UVO 0825+15 ³	8.31(21)	7.37(34)	7.51(25)	–	< 7.0	–	–	–	–	6.24(06)	–	5.49(18)
LS IV–14°116 ⁴	–	< 6.0	< 6.5	< 7.0	< 6.8	–	–	–	–	6.28(12)	–	–
HE 1256–2738 ⁵	–	–	–	–	–	–	–	–	–	–	–	6.39(23)
HE 2359–2844 ⁵	–	–	–	–	–	–	–	–	–	–	–	5.64(16)
JL 87 ⁶	–	–	–	–	–	–	–	–	–	–	–	–
cool sdB ^{2,b}	–	6.30(35)	7.10(36)	–	7.58(20)	–	–	–	–	–	–	–
warm sdB ^{2,c}	7.98(25)	7.04(36)	7.78(20)	–	7.46(24)	–	–	–	–	–	–	–
Feige 66 ⁷	8.09(20)	6.96(22)	6.37(22)	–	6.46(17)	–	–	–	–	5.21(05)	–	4.7
Sun ⁸	6.34	4.95	3.93	5.64	7.50	4.99	6.22	4.19	3.04	3.65	2.04	1.75

Notes:

a. This paper; abundances from spectral synthesis χ^2 minimization.*b.* $25 \leq T_{\text{eff}}/\text{kK} \leq 27$.*c.* $35 \leq T_{\text{eff}}/\text{kK} \leq 40$ excluding PG 0909+276 and UVO 0512–08.References: 1. [Edelmann et al. \(2003\)](#), 2. [Geier \(2013\)](#), 3. [Jeffery et al. \(2017\)](#) 4. [Naslim et al. \(2011\)](#), 5. [Naslim et al. \(2013\)](#), 6. [Ahmad et al. \(2007\)](#), 7. [O’Toole & Heber \(2006\)](#), 8. [Asplund et al. \(2009\)](#); photospheric except helium (helio-seismic), neon and argon (coronal).

to measure abundances for Cr, Mn, Fe, Co, Ni, Cu, Zn, Ga, Ge, Sn, and Pb in each star. In addition, ultraviolet abundances of lighter elements are typically in agreement with the optical measurements.

We have demonstrated that both stars are enriched by 1.5 – 3 dex in heavy metals ($Z \geq 30$). The enrichment in zinc, gallium, tin and lead is consistent with ‘normal’ sdB stars [O’Toole & Heber \(2006\)](#), and not as extreme as lead in UVO 0825+15, HE 1256–2738, and HE 2359–2844. Germanium, however, is more than 1 dex enriched compared with ‘normal’ sdB stars, and similar to that seen in UVO 0825+15 and LS IV–14°116. From these measurements, we confirm that both PG 0909+276 and UVO 0512–08 have characteristics that make them distinct from both normal H-rich sdB and intermediate He-rich sdB stars. The additional iron-group elements measured from the ultraviolet confirm a picture of two extremely metal-enriched stars, even compared with ‘normal’ sdB stars. UVO 0512–08 is possibly the most iron-rich hot subdwarf known to date, though PG 0909+276

shares the low iron abundance characteristic of the lead-rich subdwarfs.

These extreme surface chemistries present a challenge for interpretation. We observed a number of discrepancies $> 2\sigma$ between abundances measured from different wavelength regions, namely for S, Ca, and V in PG 0909+276, and C, S, Ca, Fe, Co, Ni, Cu, and Pb in UVO 0512–08. Whether this is a consequence of fine-grained elemental stratification in the photosphere remains to be verified.

Meanwhile, the leading hypothesis for the extreme enrichment of all elements with $Z \geq 18$ (except iron) remains that of a highly stratified surface in which selective radiative levitation has elevated abundant species into the line-forming region of the photosphere. These elements may contribute to missing opacity from the models, as suggested by the *IUE* spectrophotometry and *HST*/*STIS* far-ultraviolet spectroscopy. Additional work is needed to identify and include the atomic data required.

There is also an urgent need to measure iron-group el-

ement abundances in other chemically peculiar hot subdwarfs, and especially in LSIV-14°116 and UVO 0825+15 where the high-resolution ultraviolet spectrum is easily accessible to *HST*/STIS.

ACKNOWLEDGMENTS

This paper is based on observations made with the NASA/ESA Hubble Space Telescope under program 13800, and recovered from the data archive at the Space Telescope Science Institute (STScI). STScI is operated by the Association of Universities for Research in Astronomy, Inc. under NASA contract NAS 5-26555.

The Armagh Observatory and Planetarium is funded by direct grant from the Northern Ireland Department for Communities. CSJ acknowledges support from the UK Science and Technology Facilities Council (STFC) Grant No. ST/M000834/1.

The authors acknowledge Aidan Kelly for work carried out for his senior sophister research project at Armagh Observatory and Trinity College Dublin in late 2015 and which provided the first indication of iron-group overabundances in PG 0909+276.

The authors thank Ulrich Heber and Heinz Edelmann for making the optical spectra of PG 0909+276 and UVO 0512-08 available.

Some of the data presented in this paper were obtained from the Mikulski Archive for Space Telescopes (MAST). STScI is operated by the Association of Universities for Research in Astronomy, Inc., under NASA contract NAS5-26555. Support for MAST for non-HST data is provided by the NASA Office of Space Science via grant NNX09AF08G and by other grants and contracts.

This research has made use of the SIMBAD database, operated at CDS, Strasbourg, France.

This work has made use of the Vienna Atomic Line Database (VALD) database, operated at Uppsala University, the Institute of Astronomy of the Russian Academy of Sciences in Moscow, and the University of Vienna, the Atomic Line List, hosted by the Department of Physics and Astronomy, University of Kentucky, and the National Institute of Standards and Technology (NIST) Atomic Spectra Database, which is hosted by the U.S. Dept of Commerce.

REFERENCES

- Aggarwal K. M., et al., 2017, Atomic Line List v2.05b21, University of Kentucky, <http://www.pa.uky.edu/~peter/newpage/>
- Ahmad A., Behara N. T., Jeffery C. S., Sahin T., Woolf V. M., 2007, *A&A*, **465**, 541
- Alonso-Medina A., Colón C., Porcher P., 2011, *Atomic Data and Nuclear Data Tables*, **97**, 36
- Asplund M., Grevesse N., Sauval A. J., 2005, in Barnes III T. G., Bash F. N., eds, *Astronomical Society of the Pacific Conference Series Vol. 336, Cosmic Abundances as Records of Stellar Evolution and Nucleosynthesis*. p. 25
- Asplund M., Grevesse N., Sauval A. J., Scott P., 2009, *ARA&A*, **47**, 481
- Behara N. T., Jeffery C. S., 2006, *A&A*, **451**, 643
- Brown T. M., Sweigart A. V., Lanz T., Landsman W. B., Hubeny L., 2001, *ApJ*, **562**, 368
- Cutri R. M., et al., 2003, *VizieR Online Data Catalog*, **2246**
- Drilling J. S., Jeffery C. S., Heber U., Moehler S., Napiwotzki R., 2013, *aap*, **551**, A31
- Edelmann H., 2003, PhD thesis, Friedrich-Alexander-Universität Erlangen-Nürnberg
- Edelmann H., Heber U., Hagen H.-J., Lemke M., Dreizler S., Napiwotzki R., Engels D., 2003, *A&A*, **400**, 939
- Geier S., 2013, *ã*, **549**, A110
- Groenewegen M. A. T., Lamers H. J. G. L. M., 1989, *A&AS*, **79**, 359
- Han Z., 1998, *MNRAS*, **296**, 1019
- Heber U., 2016, *PASP*
- Høg E., et al., 2000, *A&A*, **355**, L27
- Iben Jr. I., 1990, *ApJ*, **353**, 215
- Ivanova N., et al., 2013, *A&ARv*, **21**, 59
- Jeffery C. S., 1991, Newsletter on 'Analysis of Astronomical Spectra', **16**, 17
- Jeffery C. S., Starling R. L. C., Hill P. W., Pollacco D., 2001a, *MNRAS*, **321**, 111
- Jeffery C. S., Woolf V. M., Pollacco D. L., 2001b, *A&A*, **376**, 497
- Jeffery C. S., et al., 2017, *MNRAS*, **465**, 3101
- Kurucz R. L., Smith P. L., Heise C., Esmond J. R., 2016, Kurucz Database, <http://www.pmp.uni-hannover.de/cgi-bin/ssi/test/kurucz/sekur.html>
- Latour M., Fontaine G., Green E. M., Brassard P., 2015, *A&A*, **579**, A39
- Martin P., Jeffery C. S., Naslim N., Woolf V. M., 2016, *MNRAS*, submitted
- Miller Bertolami M. M., Althaus L. G., Unglaub K., Weiss A., 2008, *A&A*, **491**, 253
- Morton D. C., 1978, *ApJ*, **222**, 863
- Naslim N., Jeffery C. S., Behara N. T., Hibbert A., 2011, *MNRAS*, **412**, 363
- Naslim N., Jeffery C. S., Hibbert A., Behara N. T., 2013, *MNRAS*, **434**, 1920
- Németh P., Kawka A., Vennes S., 2012, *MNRAS*, **427**, 2180
- O'Toole S. J., 2004, *A&A*, **423**, L25
- O'Toole S. J., Heber U., 2006, *A&A*, **452**, 579
- Rauch T., Quinet P., Hoyer D., Werner K., Demleitner M., Kruk J. W., 2015, TÄijbingen Oscillator Strengths Service Form Interface, VO resource provided by the GAVO Data Center, [doi:10.21938/3i01ismuCODnhzjbcvuwA](https://doi.org/10.21938/3i01ismuCODnhzjbcvuwA), <http://dc.zah.uni-heidelberg.de/toss/q/legacy/info>
- Saio H., Jeffery C. S., 2002, *MNRAS*, **333**, 121
- Schöning T., Butler K., 1989, *A&AS*, **78**, 51
- Zacharias N., et al., 2009, *VizieR Online Data Catalog*, **1315**
- Zhang X., Jeffery C. S., 2012, *MNRAS*, **419**, 452

This paper has been typeset from a $\text{\TeX}/\text{\LaTeX}$ file prepared by the author.